Supplementary information

Influence of alkaline-earth metal substitution on structure, electrical conductivity and oxygen transport properties of perovskite-type oxides $La_{0.6}A_{0.4}FeO_{3-\delta}$ (A = Ca, Sr and Ba)

Jia Song,[a] De Ning[b] and Henny. J.M. Bouwmeester[a]

[a] Electrochemistry Research Group, Membrane Science and Technology, MESA+ Institute for Nanotechnology, University of Twente, P.O. Box 217, 7500 AE, Enschede, The Netherlands

[b] Helmholtz-Zentrum Berlin für Materialien und Energie, Hahn-Meitner-Platz 1, 14109 Berlin, Germany

Table S1. Structural data of LCF64, LSF64 and LBF64 from Rietveld refinements of room-temperature XRD data. The numbers in parentheses denote standard deviations in units of the least significant digits.

Atom	Site	x	y	z	B	occ
$La_{0.6}Ca_{0.4}FeO_{3-\delta}$	*Pnma*, *a* = 5.5138(1) Å, *b* = 7.7574(1) Å, *c* = 5.4896(1) Å					
La	4c	0.0215(1)	0.25	0.9991(12)	0.86(1)	0.6
Ca	4c	0.0215(1)	0.25	0.9991(12)	0.86(1)	0.4
Fe	4b	0.5	0	0	1.16(2)	1
O1	4c	0.2806(15)	0.0142(11)	0.7267(18)	0.09(9)	2
O2	8d	0.4939(17)	0.25	0.1391(18)	7.0(3)	1
$La_{0.6}Sr_{0.4}FeO_{3-\delta}$	$R\bar{3}c$, *a* = *b* = 5.52260(6) Å, *c* = 13.4462(2) Å					
La	4c	0	0	0.25	1.7002(3)	0.6
Sr	4c	0	0	0.25	1.7002(3)	0.4
Fe	4b	0.3333	0.6667	0.1667	1.5771(7)	1
O	4c	0.5468(11)	0	0.25	1.2295(18)	3
$La_{0.6}Ba_{0.4}FeO_{3-\delta}$	$Pm\bar{3}m$, *a* = *b* = *c* = 3.92652(2) Å					
La	4c	0	0	0	2.41(2)	0.6
Ba	4c	0	0	0	2.41(2)	0.4
Fe	4b	0.5	0.5	0.5	2.28(4)	1
O	4c	0.5	0.5	0	3.57(9)	3

Table S2. Activation energies of D_{chem} and k_{chem} of LCF64, LSF64 and LBF64 extracted from data of ECR experiments, following pO_2 step changes 0.21 → 0.1 atm (Red) and 0.1 → 0.21 atm (Ox).

Materials	D_{chem}		k_{chem}	
	Red	Ox	Red	Ox
	E_a (kJ mol^{-1})	E_a (kJ mol^{-1})	E_a (kJ mol^{-1})	E_a (kJ mol^{-1})
LCF64	98 ± 2	97 ± 1	146 ± 2	144 ± 1
LSF64	93.6 ± 0.4	93.9 ± 0.4	86 ± 1	82 ± 1
LBF64	88.8 ± 0.2	89.8 ± 0.4	92 ± 1	83.3 ± 0.7

Table S3. Activation energies of D_s of LCF64, LSF64 and LBF64 extracted from data of ECR experiments, following pO_2 step changes 0.21 $\rightarrow$ 0.1 atm (Red) and 0.1 $\rightarrow$ 0.21 atm (Ox).

Materials	D_s	
	Red	Ox
	E_a (kJ mol^{-1})	E_a (kJ mol^{-1})
LCF64	139 ± 2	138 ± 2
LSF64	143 ± 1	145 ± 1
LBF64	103 ± 1	106 ± 1

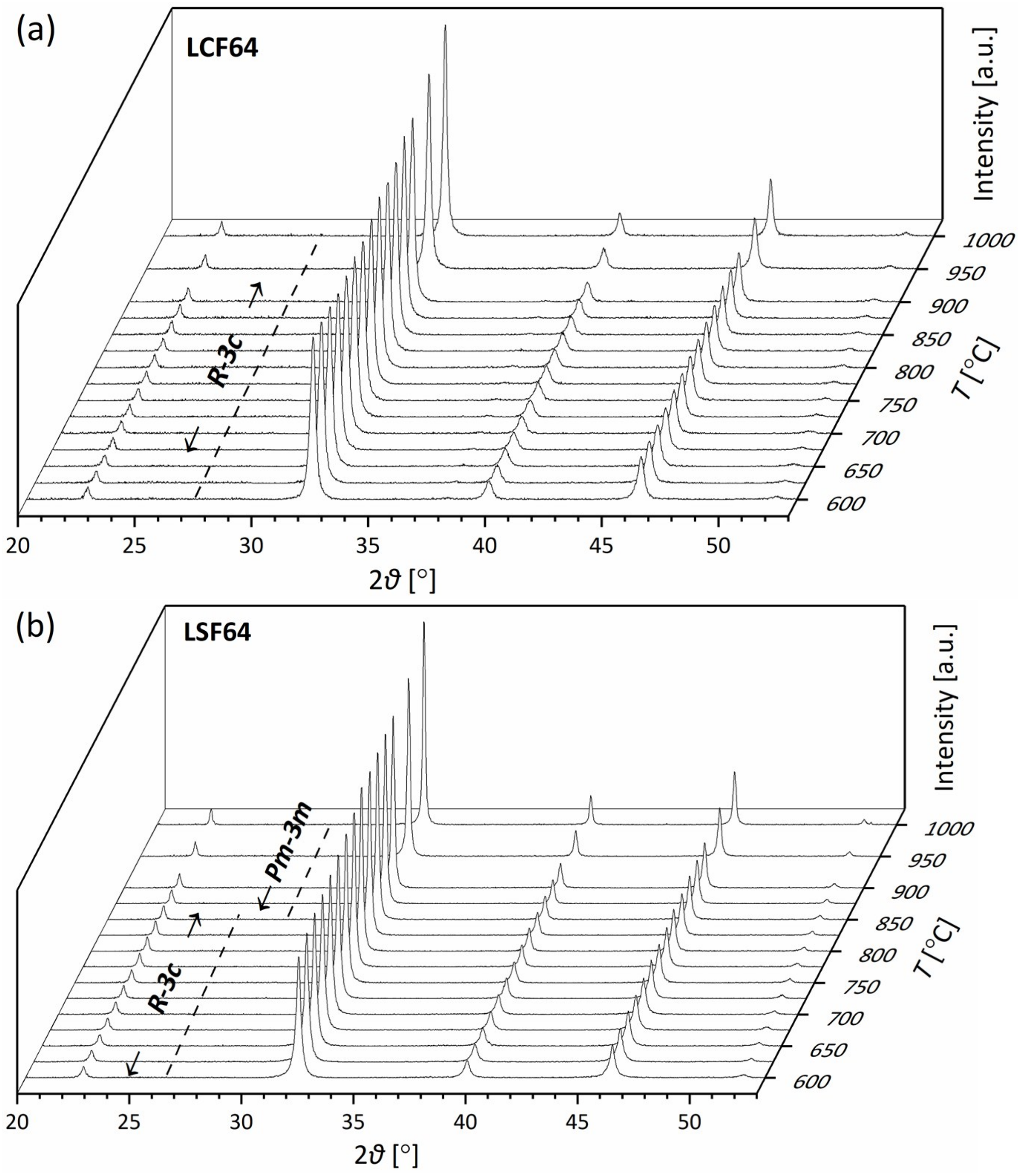
(a)
LCF64
Intensity [a.u.]
R-3c
T [°C]
1000
950
900
850
800
750
700
650
600
20
25
30
35
40
45
50
2ϑ [°]
(b)
LSF64
Intensity [a.u.]
Pm-3m
R-3c
T [°C]
1000
950
900
850
800
750
700
650
600
20
25
30
35
40
45
50
2ϑ [°]

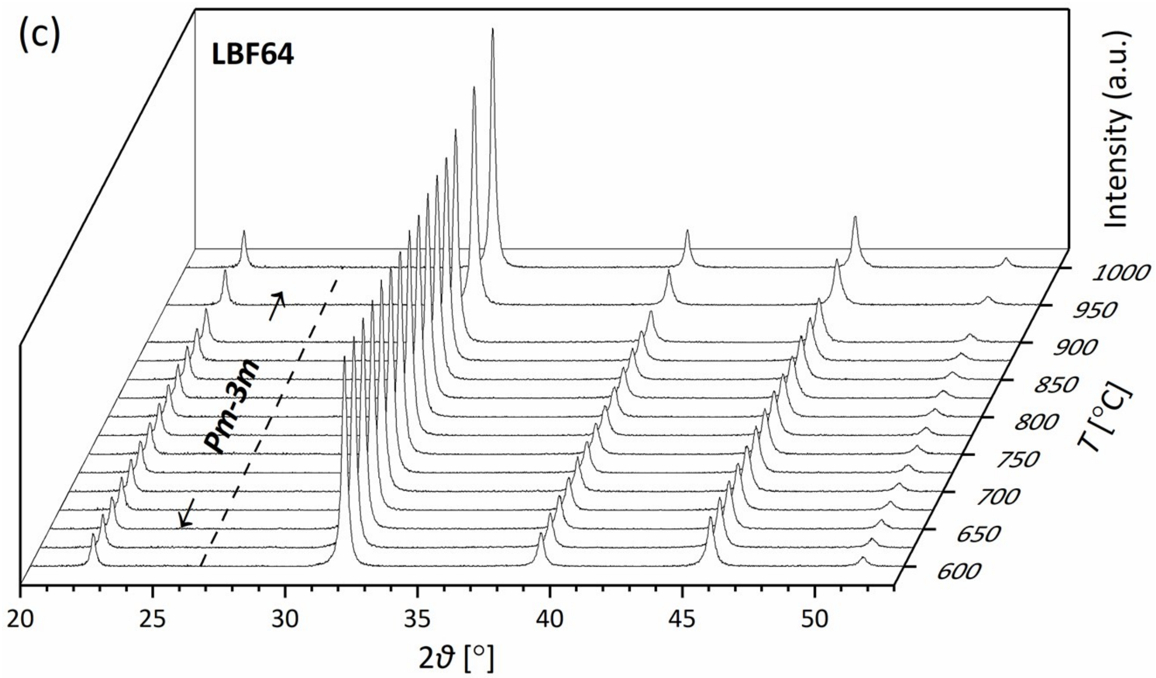

Fig. S1 *In situ* high temperature XRD patterns for (a) LCF64, (b) LSF64, and (c) recorded between 20° and 56° in air.

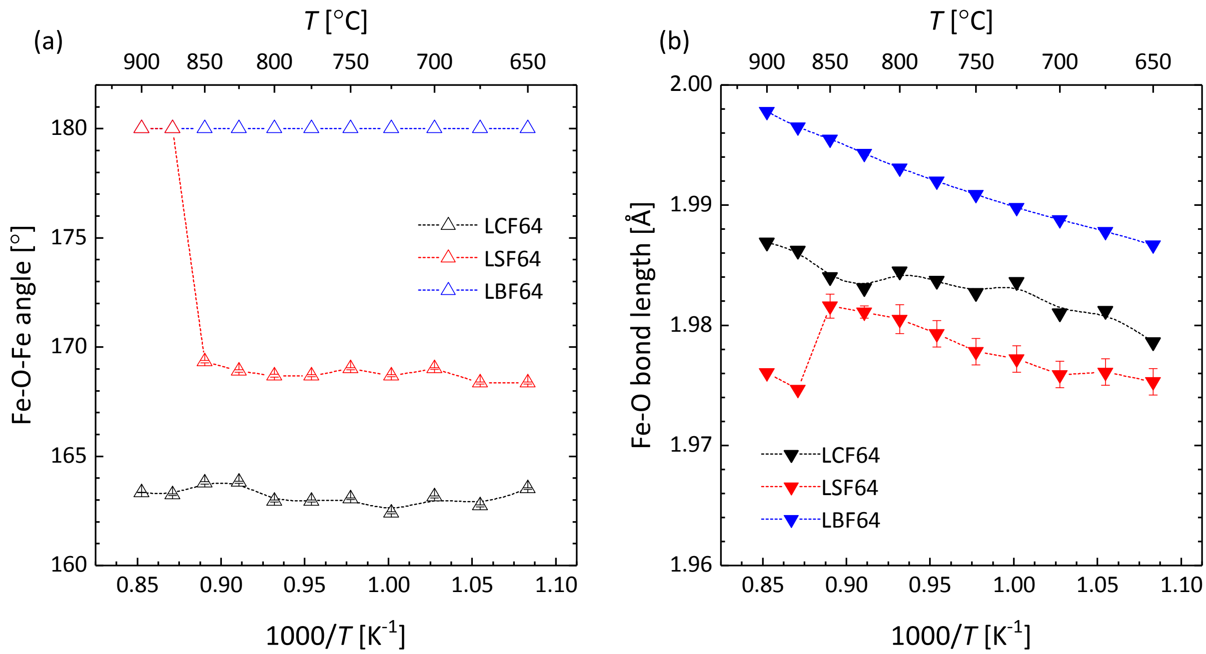

Fig. S2 (a) Fe-O-Fe angle and (b) Fe-O bond distance for LCF64, LSF64 and LBF64 obtained from Rietveld refinements of HT-XRD patterns recorded in ambient air.

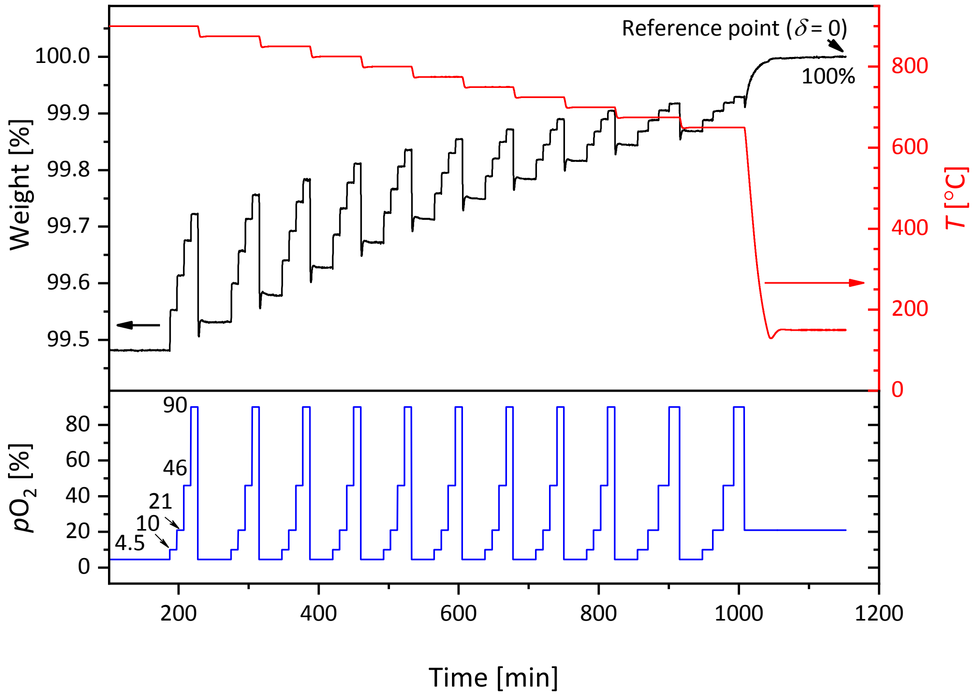

Fig. S3 Typical measurement scheme used for thermogravimetric analysis.

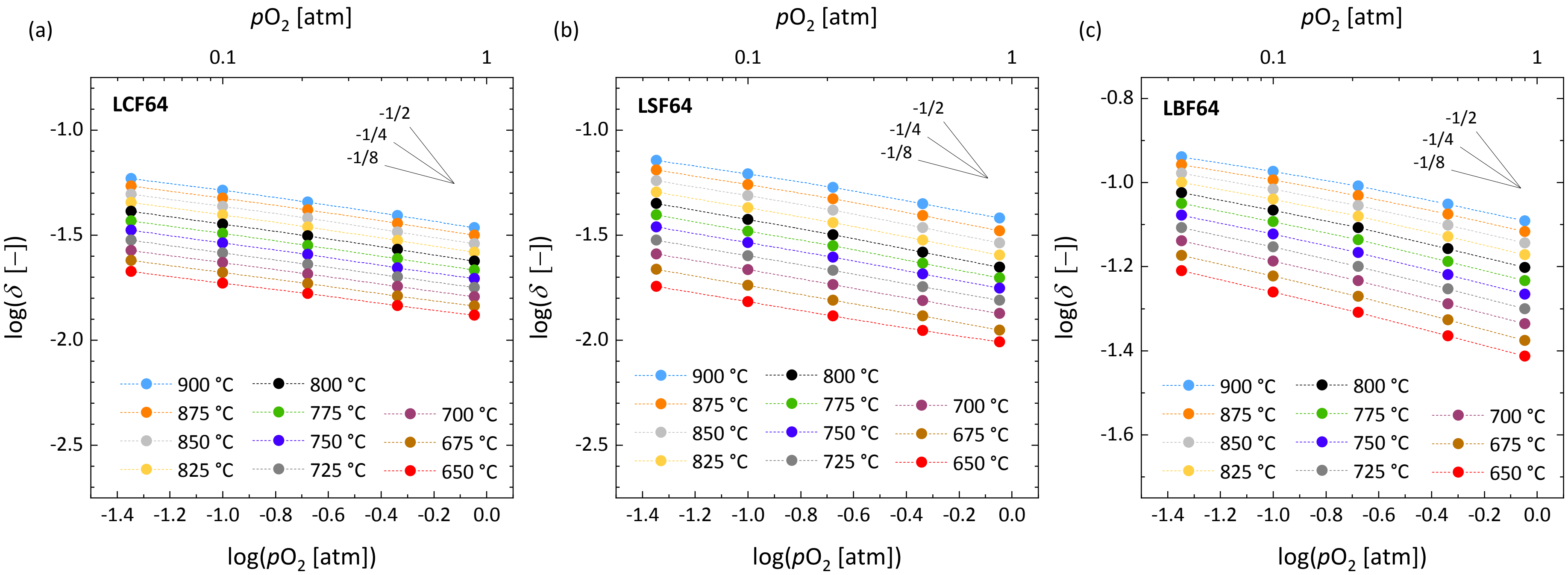

Fig. S4 Plots of log(δ) *vs* log(pO_2) for (a) LCF64, (b) LSF64 and (c) LBF64 derived from data of thermogravimetry.

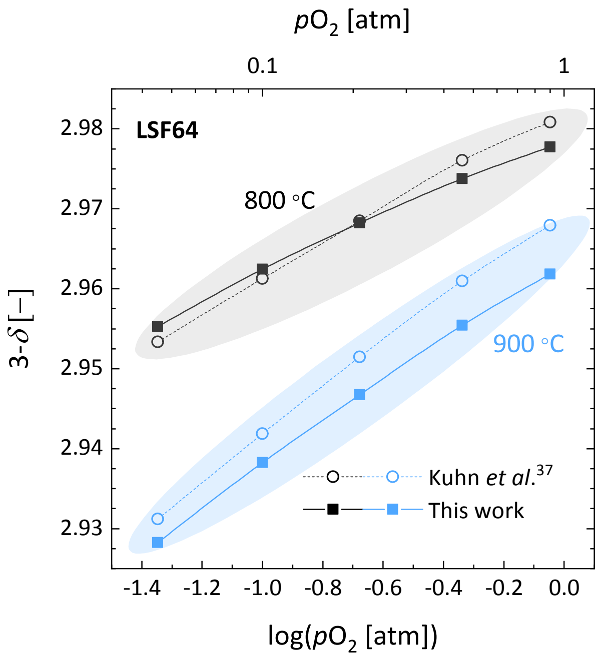

Fig. S5 Comparison of the data of oxygen stoichiometry (3-δ) at 800 °C and 900 °C for LSF64 from this study with corresponding data obtained by Kuhn *et al.*[37] Lines are drawn to guide the eye.

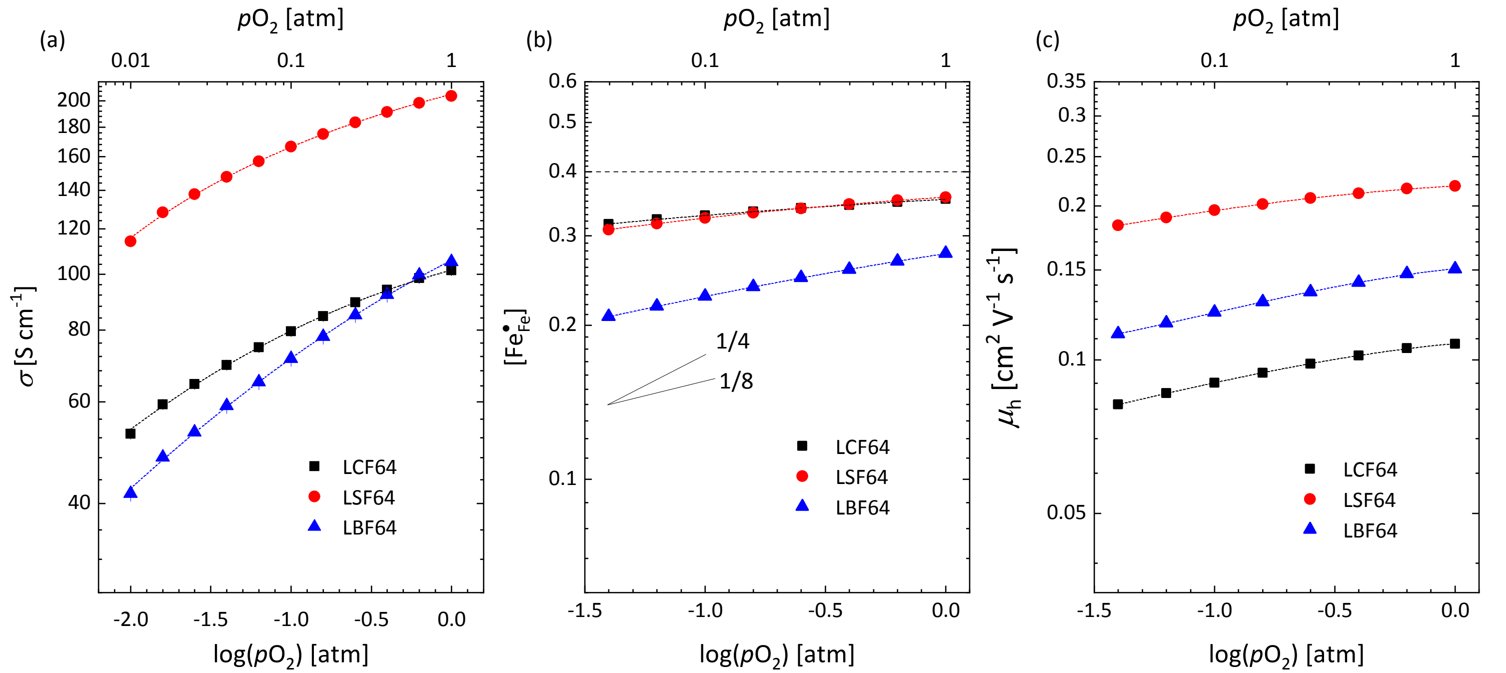

Fig. S6 pO_2 dependence of the (a) electrical conductivity, (b) defect concentration $[Fe^{\bullet}_{Fe}]$ and (c) mobility of electron-holes, at 800 °C, for LCF64, LSF64 and LBF64. The dashed lines through the data points are drawn to guide the eye. The horizontal line in (b) represents the $[Fe^{\bullet}_{Fe}]$ concentration when electronic compensation is predominant, noting that all three materials have the same concentration of the alkaline-earth metal dopant (*cf*. Eq. 7).

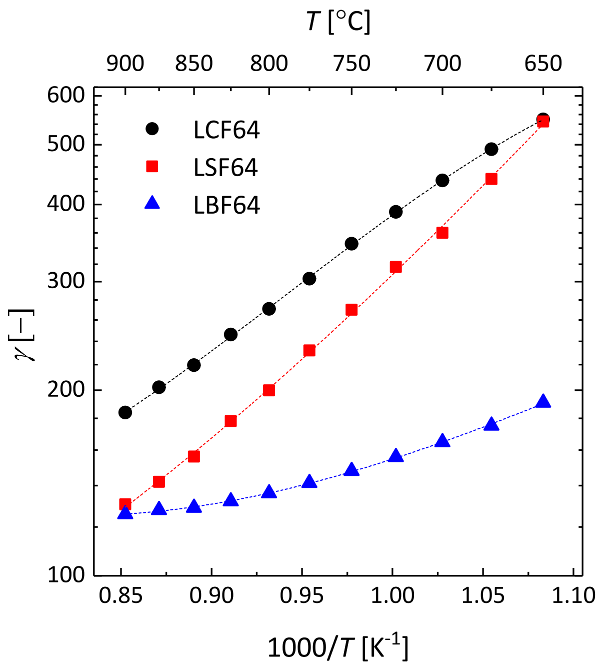

Fig. S7 Inverse temperature dependence of the thermodynamic factor for LCF64, LSF64 and LBF64 calculated from data of thermogravimetry obtained at pO_2 = 0.1416 atm. The specified pO_2 corresponds to the logarithmic average of the initial and final values of the pO_2 step change during ECR experiments.